


Article

Corrosion Behaviour and J774A.1 Macrophage Response to Hyaluronic Acid Functionalization of Electrochemically Reduced Graphene Oxide on Biomedical Grade CoCr

Belén Chico ¹, Blanca Teresa Pérez-Maceda ^{2,†}, Sara San José ², María Lorenza Escudero ¹,
María Cristina García-Alonso ^{1,*}  and Rosa María Lozano ^{2,*}

¹ Department of Surface Engineering, Corrosion and Durability, Centro Nacional de Investigaciones Metalúrgicas (CENIM, CSIC), Avda, Gregorio del Amo 8, 28040 Madrid, Spain; bchico@cenim.csic.es (B.C.); escudero@cenim.csic.es (M.L.E.)

² Cell-Biomaterial Recognition Lab., Department of Cell and Molecular Biology, Centro de Investigaciones Biológicas Margarita Salas (CIB-MS, CSIC), Ramiro de Maeztu 9, 28040 Madrid, Spain; bpm@cib.csic.es (B.T.P.-M.); sara.sanjose@urjc.es (S.S.J.)

* Correspondence: crisa@cenim.csic.es (M.C.G.-A.); rlozano@cib.csic.es (R.M.L.); Tel.: +34-915-538-900 (M.C.G.-A.); +34-918-373-112 (R.M.L.)

† Dr. Blanca Teresa Pérez-Maceda who participated actively in this research with great enthusiasm has passed away.



Citation: Chico, B.; Pérez-Maceda, B.T.; San José, S.; Escudero, M.L.; García-Alonso, M.C.; Lozano, R.M. Corrosion Behaviour and J774A.1 Macrophage Response to Hyaluronic Acid Functionalization of Electrochemically Reduced Graphene Oxide on Biomedical Grade CoCr. *Metals* **2021**, *11*, 1078. <https://doi.org/10.3390/met11071078>

Academic Editor: Krzysztof Rokosz

Received: 1 June 2021

Accepted: 29 June 2021

Published: 5 July 2021

Publisher's Note: MDPI stays neutral with regard to jurisdictional claims in published maps and institutional affiliations.



Copyright: © 2021 by the authors. Licensee MDPI, Basel, Switzerland. This article is an open access article distributed under the terms and conditions of the Creative Commons Attribution (CC BY) license (<https://creativecommons.org/licenses/by/4.0/>).

Abstract: Improvements in the lubrication of metal–metal joint prostheses are of great clinical interest in order to minimize the particles released during wear–corrosion processes. In this work, electrochemically reduced graphene oxide (ErGO) on CoCr was functionalized with hyaluronic acid (ErGOHA). Functionalization was carried out by soaking for 24 h in phosphate buffer saline (PBS) solution containing 3 g/L hyaluronic acid (HA). The corrosion performance of CoCrErGO and CoCrErGOHA surfaces was studied by electrochemical impedance spectroscopy (EIS) for 7 days in PBS. Biocompatibility and cytotoxicity were studied in mouse macrophages J774A.1 cell line by the measurement of mitochondrial activity (WST-1 assay) and plasma membrane damage (LDH assay). The inflammatory response was examined through TNF- α and IL-10 cytokines in macrophages culture supernatants, used as indicators of pro-inflammatory and anti-inflammatory responses, respectively. EIS diagrams of CoCrErGOHA revealed two time constants: the first one, attributed to the hydration and diffusion processes of the HA layer adsorbed on ErGO, and the second one, the corrosion resistance of ErGOHA/CoCr interface. Macrophage assays showed better behavior on CoCrErGOHA than CoCr and CoCrErGO surfaces based on their biocompatible, cytotoxic, and inflammatory responses. Comparative analysis of IL-10 showed that functionalization with HA induces higher values of anti-inflammatory cytokine, suggesting an improvement in inflammatory behavior.

Keywords: hyaluronic acid; CoCr alloy; electrochemically reduced graphene oxide; macrophages; corrosion; inflammatory response

1. Introduction

Cobalt–chromium (CoCr) alloy is one of the most commonly used materials for joint replacements [1,2]. The durability of joint replacements, such as cobalt–chromium alloys, depends mainly on the wear–corrosion processes. CoCr alloys are covered by a passive film protecting the surface but irretrievably undergo wear–corrosion phenomena, causing debris and metallic dissolution. Wear particles and metal ions from prosthetic devices may induce a cascade of adverse cellular reactions that may include inflammatory complications, macrophage activation, bone resorption, and rarely, neoplasia [3,4]. In this context, macrophages play a decisive role in the hostile inflammatory reactions, the biocompatibility and cytotoxicity, that can lead to the loosening and failure of the implants [4,5]. Therefore,

it is essential to find new strategies in order to increase lubrication and minimize the wear process.

The characterization of the surface of retrieval metal-on-metal joint replacements has revealed tribological films composed of graphitic compounds in areas where sliding takes place [6–8]. These findings have raised questions about the possibilities of integrating carbon-base compounds on the surface of biomedical implants prior to their implantation. The discovery of graphitic compounds on the prosthesis surface has induced the proposal of using graphene compounds deposited onto the metallic surfaces in order to improve their tribocorrosion properties. Several works in literature deal with the exceptional properties of graphene derivative used as a solid lubricant, emulating the good performance of graphite in humid environments in industrial applications.

The main handicap of covering the prosthesis with graphene is to find the best procedure to uniformly deposit the surface. At this point, the use of a graphene oxide dispersion as a precursor is a convenient smart pathway to obtain graphene-enriched surfaces. Graphene oxide (GO) incorporates oxygen atoms into the carbon network, adding hydroxyl and epoxy groups on its basal plane and carboxyl groups on the edges [9]. The reduction of graphene oxide (GO) on metal substrates can be assured by several techniques, such as chemical or electrochemical methods, of low cost of synthesis and easy deposition. Total reduction of GO usually does not happen, and oxygen atoms in the carbon structure facilitate the functionalization with other substances. The importance of studying the surface modification with graphene-based structures is because of the great interest in decreasing corrosion and enhancing the wearability of implants [10].

To the best of our knowledge, there has only been one study recently published by our group on the electrochemical reduction of graphene oxide on CoCr-based alloys [11]. As was reported in [12], the electrochemical deposition of reduced graphene oxide (ErGO) on a biomedical grade CoCr produced a considerable increase in the macrophages' biocompatibility.

To increase the biocompatibility of the ErGO deposited on the CoCr surfaces, the additional functionalization of CoCrErGO with hyaluronic acid, the main lubricant component of the synovial fluid in the articular joints [13], has been studied here. Therefore, the main objective of this paper is the study of the HA functionalization of the ErGO on the CoCr alloy from the point of view of corrosion and biological implications. Since macrophages are the main cells involved in the primary response to foreign bodies [14], the response of a mouse macrophage cell line (J774A.1) was analyzed here [15].

2. Materials and Methods

2.1. Materials

The biomedical grade CoCr alloy used for this study was provided by International Edge with the following chemical composition (wt.%): 27.25% Cr, 5.36% Mo, 0.69% Mn, 0.68% Si, 0.044% C, 0.02% W, 0.15% N, 0.002% Al, 0.001% S, 0.002% P, 0.002% B, 0.001% Ti, balance Co.

CoCr discs of 12 mm diameter and 2 mm thickness were used. They were roughened on successive abrasive papers in silicon carbide grade from 600 to 2000 and subsequently washed with distilled water.

2.2. Functionalization of Electrochemically Reduced Graphene Oxide with Hyaluronic Acid

2.2.1. Electrochemical Reduction of Graphene Oxide (ErGO)

Immediately after grinding, direct electrochemical reduction of the graphene oxide contained in an aqueous solution (4 g/L) was performed on the CoCr surfaces. The electrochemical method used to synthesize the reduced graphene oxide films on CoCr surfaces was cyclic voltammetry (CV), from -2.1 to -0.5 V Ag/AgCl at a scanning rate of 10 mV/min for 5 cycles [11]. Electrochemical tests were performed in a three-electrode electrochemical cell where the two-side CoCr discs were the working electrode, while graphite bars placed in front of each CoCr side were the auxiliary electrode and the Ag/AgCl electrode was used as the reference electrode.

2.2.2. Functionalization with Hyaluronic Acid

The electrochemically reduced graphene oxide (ErGO) deposited on the CoCr surfaces was washed with distilled water and further functionalized with hyaluronic acid (hyaluronic acid, 53747, Sigma-Aldrich Chemie GmbH, Schnelldorf, Germany), hereafter named ErGOHA. Functionalization was carried out by soaking CoCrErGO samples for 24 h in a phosphate buffer saline (PBS) solution of chemical composition: 0.2 g/L KCl, 0.2 g/L KH_2PO_4 , 8 g/L NaCl, and 1.150 g/L Na_2HPO_4 anhydrous, and containing 3 g/L of hyaluronic acid (HA), the concentration equivalent of that found in the synovial fluid [13].

2.2.3. Electrochemical Characterization of ErGO and ErGOHA on CoCr

The corrosion behavior of CoCrErGOHA, CoCrErGO, and CoCr surfaces in PBS solution was assessed by the measurement of the open circuit potential and electrochemical impedance spectroscopy (EIS) for 7 days. This potential was measured with respect to the saturated calomel electrode with the time without any electric perturbation.

A Gamry 600 potentiostat (Gamry Instruments, Warminster, PA, USA) was used to carry out the electrochemical measurements. The impedance data were obtained for the corrosion potential by applying a sinusoidal wave of 10 mV in amplitude, in a frequency range from 100 kHz to 1 mHz, logarithmically spaced by 5 points/decade. All the electrochemical experiments were performed in triplicate with a working area of 78.5 mm².

The impedance response was analyzed by fitting the experimental data with the proper equivalent circuit model. The elements of the equivalent circuit were estimated by using a non-linear least-squares program (NLLS program) included in Z-view software for all the CoCr surfaces. The criteria used in estimating the quality of the fitting were, firstly, the lowest chi-square value, and, secondly, the lowest relative errors (in %) for all the fitted values.

2.3. Biocompatibility Response—Macrophages Cultures Assays

Prior to the cell culture assays, both sides of the metallic discs were sterilized for 5 min under UV in an active vertical flux cabin.

Biocompatibility tests of CoCrErGOHA, CoCrErGO, and CoCr of 12 mm diameter discs were evaluated in the mouse macrophage J774A.1 cell line provided by DSMZ Human and Animal Cell Bank (DSMZ, Braunschweig, Germany).

The effect of the modified surfaces on the proliferation, biocompatibility, and cytotoxicity of cell cultures was analyzed by seeding macrophages at 25,000 cells/mL on 24-well culture plates in a volume of 1 mL complete cell culture medium (Dulbecco's Modified Eagle Medium, DMEM 41966; Gibco ThermoFisher Scientific, Waltham, MA, USA) supplemented with 10% heat-inactivated fetal bovine serum (FBS; Gibco ThermoFisher Scientific, Waltham, MA, USA) and with a mixture of antibiotics (penicillin at 100 units/mL and streptomycin at 100 µg/mL, Gibco, BRL) that was used as a culture medium. Cell cultures were maintained for 72 h in a cell culture chamber at 37 °C and 5% CO₂. Incubation time selected was based on the previous set-up of cell cultures assays for metallic material studies performed in the lab, that is, the most common time point used for cell viability studies [15,16].

Mitochondrial activity (WST-1 assay) and plasma membrane damage (LDH assay) were used to evaluate the biocompatibility and cytotoxicity, respectively, as described in [17].

2.3.1. Cell Fixation and Optical Microscopy

To carry out the morphological studies and visualize the proliferation of macrophages cultured on CoCrErGOHA, CoCrErGO, and CoCr discs for 72 h, the macrophages were directly fixed on the culture plate with 1 mL of cold methanol and incubated for 10 min at −20 °C followed by two 5 min wash-step with PBS. Finally, the discs were maintained at 4 °C in 1 mL of PBS.

2.3.2. Measurement of Mitochondrial Activity

Reduction of the WST-1 reagent (4-[3-4-iodophenyl]-2-(4-nitro-phenyl)-2H-5-tetrazolio]-1,3-benzene disulfonate (Roche Diagnostics GmbH, Mannheim, Germany) was used to evaluate the effect of modified surfaces on the mitochondrial activity of macrophages. The mitochondrial activity measurement is directly proportional to the number of metabolically active cells in culture [15]. After 72 h in culture, 100 μ L of the cell proliferation kit reagent WST-1 was added to each well containing 1 mL of fresh complete cell culture medium, and the mixture was incubated inside the cell culture incubator for 90 min. After incubation, 100 μ L of each reaction mixture was transferred to a 96-wells cell plate, and the absorbance of the samples was measured as differential absorbance, 415 minus 655 nm, in an iMark microplate absorbance reader (Bio-Rad, Richmond, CA, USA), using the absorbance given by complete cell culture medium as a control. All experiments were carried out independently and in triplicate, and data are expressed as means \pm standard deviations.

2.3.3. Measurement of Lactate Dehydrogenase Activity

To measure and quantify the effect of modified materials on the cell death and cell lysis, lactate dehydrogenase (LDH) activity was measured in the supernatants of cell cultures with an enzymatic assay using the Cytotoxicity Detection Kit^{plus} (Roche Diagnostics GmbH, Mannheim, Germany). Supernatants were collected from cell culture after being exposed for 72 h to the different materials and were centrifuged for 5 min at 1024 \times g. The enzymatic assays were performed according to the LDH kit protocol provided by Roche Diagnostics. Complete cell culture medium was used as a control for the absorbance baseline. LDH activity was measured based on differential absorbance, 490 minus 655 nm, in an iMark microplate absorbance reader (Bio-Rad, Richmond, CA, USA). LDH catalyzes the conversion of lactate to pyruvate, reducing NAD^+ to NADH/H^+ , which is used by the catalyst to reduce a tetrazolium salt to a formazan salt, which is responsible for the change in absorbance at 490 nm. Quantification of LDH activity is used as an indicator of plasma membrane damage, as it is a stable cytoplasmic enzyme present in all cells and rapidly released into the cell culture supernatant when the plasma membrane is damaged, which is a sign of cell death [17]. All experiments were carried out as independent triplicate, and data are expressed as means \pm standard deviations.

To measure the macrophage biocompatibility of CoCrErGOHA, CoCrErGO, and CoCr discs, a ratio between LDH/WST-1 values was employed to relate plasma membrane damage to the number of metabolically active cells in culture [12].

2.3.4. Inflammatory Response of J774A.1 Macrophage to CoCrErGOHA, CoCrErGO, and CoCr

To evaluate the inflammatory response of J774A.1 macrophages to the modified surfaces, the concentration of pro-inflammatory ($\text{TNF-}\alpha$) and anti-inflammatory (IL-10) cytokines were measured in supernatants of macrophages in culture with the metallic materials for 72 h.

After culture, cell supernatants were collected and centrifuged for 5 min at 1024 \times g. The measurement of cytokines was performed with commercial kits specifically for detection of $\text{TNF-}\alpha$ (Murine $\text{TNF-}\alpha$ Elisa Kit, Diaclone, Besançon Cedex, France) and IL-10 (Murine IL-10 Elisa Kit, Diaclone, Besançon Cedex, France) following the indications given by the commercial brochure.

To assess the reproducibility of data, results were from three independent experiments, and each assay was carried out with six replicates for each metallic material in the study. Data are expressed as means \pm standard deviations.

2.3.5. Statistical Analysis of the Biocompatibility and Inflammatory Response Assays

Differences between groups were tested with a one-way analysis of variance. For those cases where differences were significant (p value ≤ 0.05), mean pairwise comparisons

were computed with a Tukey's test. All analyses were performed with the R software version 3.6.3 (R Core Team) [18].

3. Results and Discussion

The CoCr alloys have numerous applications as biomedical implants, such as femoral heads or coronary stents. In both types of application, the materials offer advantages as well as disadvantages, depending on their surface conditions. The improvement of the surface performance with different treatments and/or coatings on CoCr alloys has been widely reported in the scientific bibliography. The use of coatings introduces the risk of coating defects such as cracks or peeling that, in the specific case of femoral heads, cause a significant increase in the wear rate. Research should be based on investigating the surface functionalization in order to minimize wear processes. In trauma applications, the increase in lubrication in the replaced joints is extremely important. Bearing this in mind and knowing that hyaluronic acid is the main lubricant component of the synovial fluid, this paper deals with the functionalization with HA of ErGO, deposited as a solid lubricant, which is an additional step in the modification and improvement of the CoCr articular surfaces [11,12].

The electrochemical response to this surface modification on CoCr in physiological medium PBS is represented in Figures 1 and 2. Figures 1 and 2 show the Nyquist (a) and Bode (b) diagrams for CoCrErGOHA, CoCrErGO, and CoCr surfaces at 0 days and after 7 days of immersion in PBS, respectively.

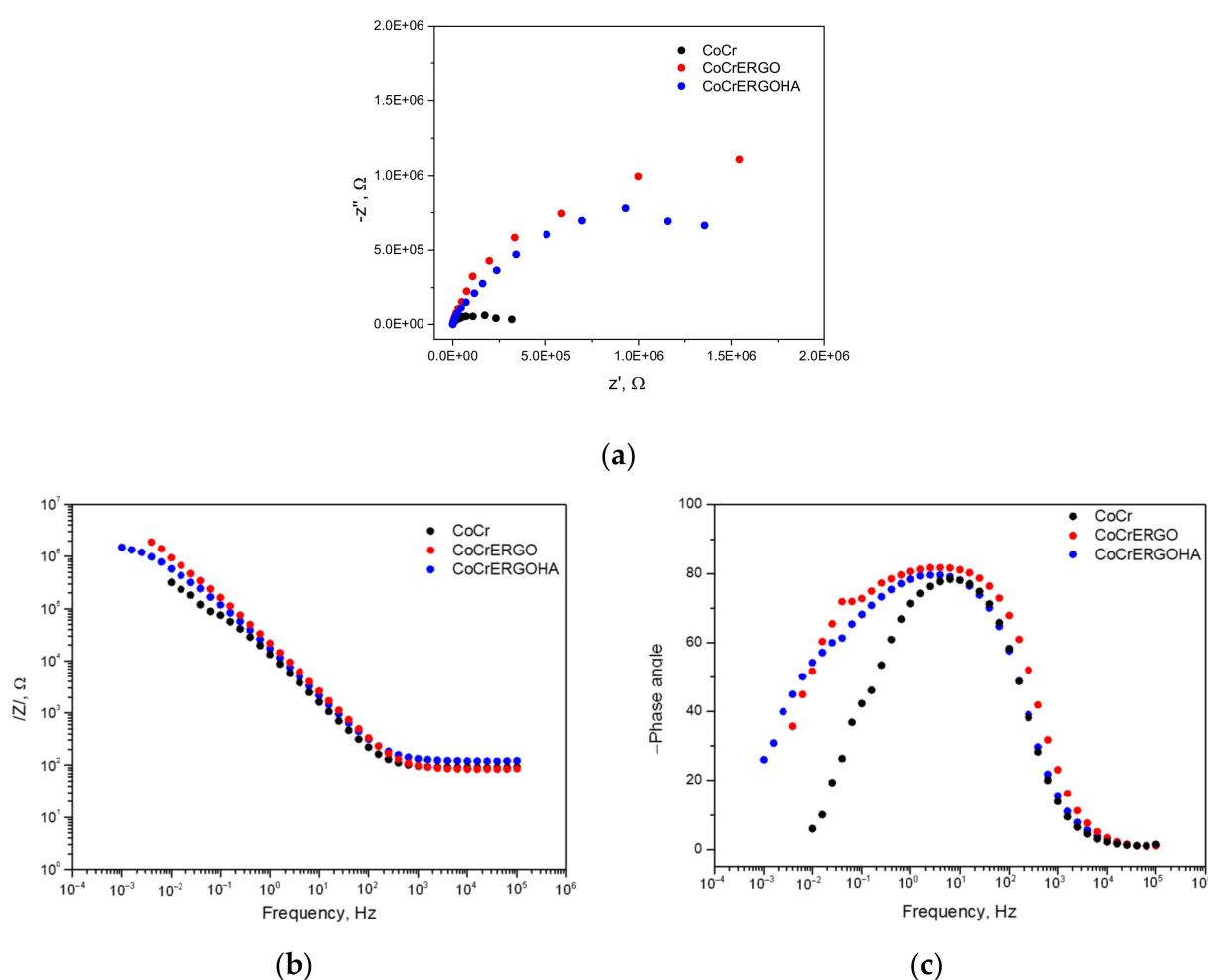


Figure 1. Nyquist diagrams (a) and Bode diagrams of impedance modulus (b) and phase angle (c) versus frequency, for CoCr, CoCrErGO, and CoCrErGOHA surfaces at 0 days of immersion in PBS.

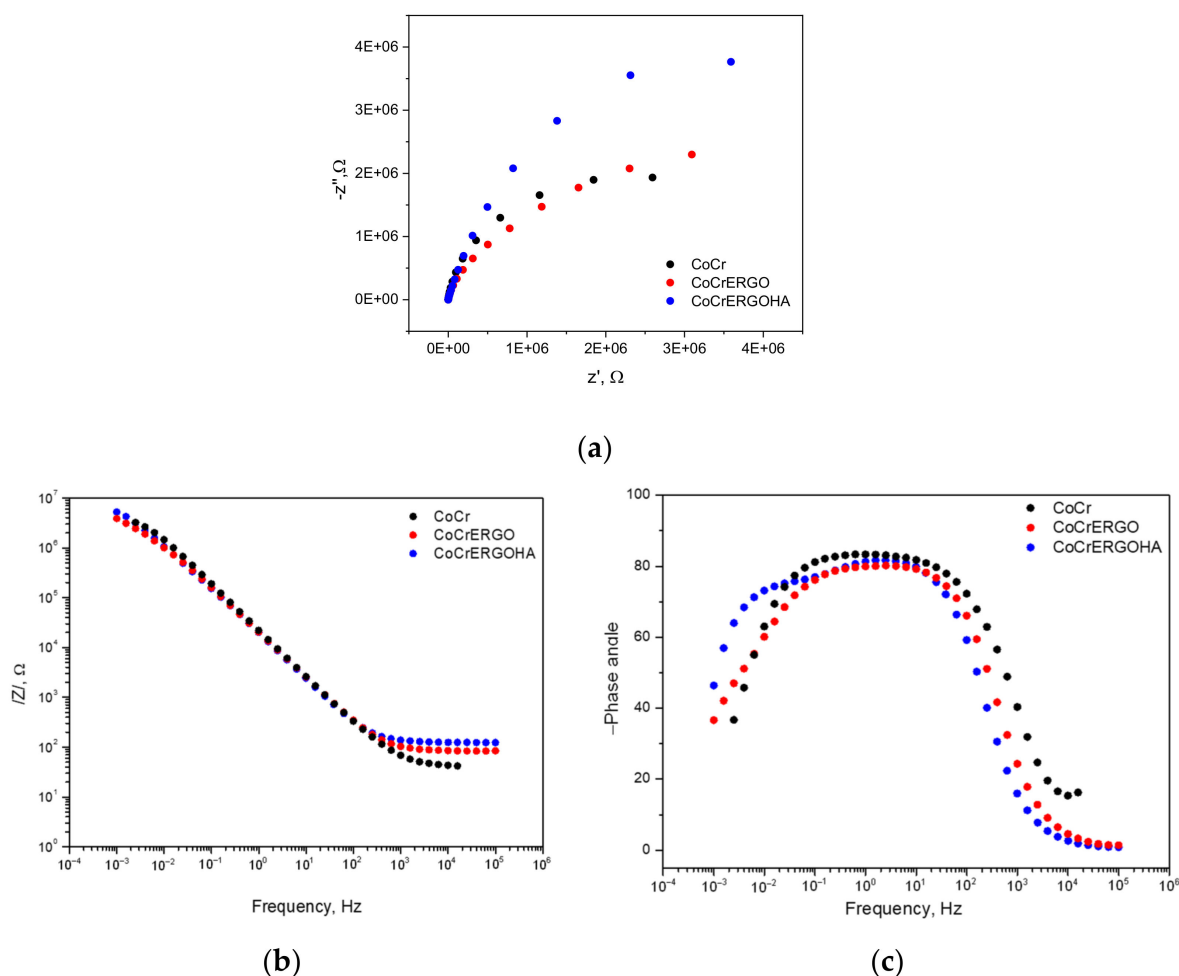


Figure 2. Nyquist diagrams (a) and Bode diagrams of impedance modulus (b) and phase angle (c) versus frequency, for CoCr, CoCrErGO, and CoCrErGOHA surfaces after 7 days of immersion in PBS.

The measurements of EIS at 0 days were carried out once the stabilization of the corrosion potential was achieved. The Nyquist diagrams (Figure 1a) at the first times of immersion show semicircles whose shape and diameter amplitude depend on the surface modification. In fact, the impedance response of bare CoCr surfaces describes a depressed semicircle, indicating that the CoCr alloys have a native oxide layer of a few nm on the surface, which is spontaneously formed and provides good corrosion resistance. The corrosion process is controlled by this passive layer through which an activation mechanism associated with a charge transfer process takes place. CoCr surfaces covered by ErGO and ErGOHA films show an open arc semicircle of higher diameter that reveals that the corrosion process is slowed down, probably due to a barrier film. The Bode diagrams show that the impedance modulus is higher for CoCr surfaces covered with ErGO and ErGOHA (Figure 1b) and that the phase angles draw only one maximum for the CoCr surface, which is indicative of only one time constant (Figure 1c). On the other hand, a shoulder in the phase angle at the lowest frequencies appears for ErGO and ErGOHA surfaces, ascribed to a probable second time constant in the electrochemical process. However, the fitting with two time constants was not possible for ErGO surface according to the criteria used in estimating the quality of the fitting.

The phase angle values remain within the values near -90 (between 0.1 and 100 Hz) for ErGO and ErGOHA surfaces at a wider frequency range than on bare CoCr surfaces (around 10 Hz).

After 7 days of immersion in PBS, in the Nyquist diagram, all the surfaces show semicircular arcs of high amplitude (Figure 2a). In the case of bare CoCr surfaces, the

passive film improves the response to the corrosion process over time. However, this effect is clearer on ErGOHA surfaces, indicating that there is greater protection against the corrosive medium, which could be due to increased hydration capture by the HA molecules. The impedance modulus values in the Bode diagram (Figure 2b) are similar for the three surfaces under study. However, the phase angle values (Figure 2c) in ErGOHA surfaces again show a shoulder at the lowest frequency values, which indicates that the second time constant is playing a role in the electrochemical process. This time constant is due to the presence of HA on the ErGO surfaces and is attributed to the processes and phenomena that could be taking place through the hyaluronic acid adsorbed, such as water uptake, diffusion of species, and adsorption/desorption of substances. This fact provides evidence for the high sensitivity of the measurement of the phase angle for analyzing subtle yet perceptible possible changes in the electrochemical system.

The experimental impedance data have been fitted to equivalent electrical circuits considering one time constant (simple Randles circuit, Figure 3a) or two time constants (Figure 3b) in order to understand the experimental impedance response of each modified surface during the testing time on the basis of passive electrical elements. These two equivalent circuits proposed are adequate for explaining passive metal/electrolyte and ErGO or ErGOHA films on passive metal/electrolyte systems, respectively.

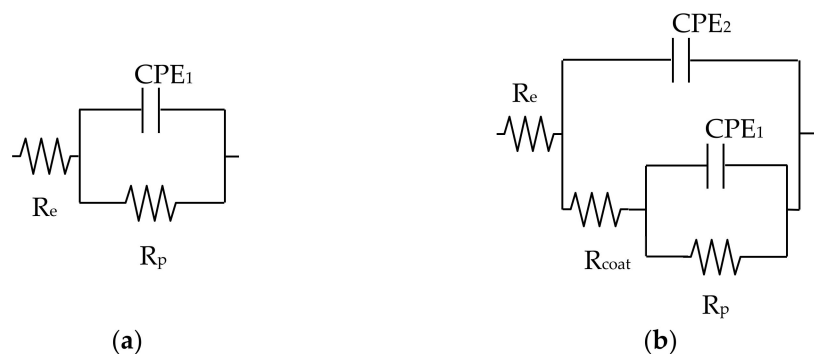


Figure 3. Equivalent circuits used for the fitting of the impedance response of CoCr, CoCrErGO, and CoCrErGOHA surfaces during testing times considering one constant time (a) and two constant times (b).

The electrical components used to fit the impedance data in the equivalent circuits (Figure 3a,b), are R_e , which is the electrolyte resistance, and CPE_1 and R_p , which are the constant phase element and the resistance linked with the time constant associated with the metallic surface/electrolyte electrochemical interface (Figure 3a). On the other hand, in Figure 3b, in addition to the previous elements, there appears a new constant phase element and the ionic resistance, i.e., CPE_2 and R_{coat} , linked to a second time constant due to the electrochemical response of the films deposited on the CoCr surface (CoCrErGO and CoCrErGOHA) in contact with the electrolyte.

The fitting results for the CoCrErGOHA, CoCrErGO, and CoCr surfaces appear in Table 1.

The equivalent circuit model represented in Figure 3a has been used for the fitting of the experimental impedance values of CoCr surfaces at 0 and 7 days and CoCrErGO surfaces at 0 days of immersion in PBS, defined by CPE_1 and R_p . The equivalent circuit model represented in Figure 3b has been used for fitting CoCrErGO at 7 days' immersion and CoCrErGOHA at 0 and 7 days' immersion in PBS that incorporates R_{coat} and CPE_2 . In this Table 1, the capacitance values, C_{CPE} , from the CPE_1 and CPE_2 (only for $n \geq 0.9$) and R values have been added, according to Equation (1) [19,20]:

$$C_{CPE} = \frac{(QR)^{\frac{1}{n}}}{R} \quad (1)$$

where Q is the constant phase element values (CPE_1 or CPE_2); R is resistance (R_p or R_{coat}), and n is exponent $n \geq 0.9$.

Table 1. Fitting values of the experimental impedance data by using the equivalent circuits of Figure 3. R_e —electrolyte resistance; CPE_1 —constant phase element and R_p —resistance related to metal surface/electrolyte interface; CPE_2 —constant phase element and R_{coat} —ionic resistance due to the films deposited on the CoCr surface. C_{exp} —experimental capacitance calculated in the high-frequency region (Equation (2)), C_{CPE1} and C_{CPE2} —capacitance calculated from CPE values (Equation (1)), only for $n \geq 0.9$.

Surface	Time, d	$R_e \pm$ Error %, Ω	$R_{coat} \pm$ Error %, $M\Omega$	$CPE_2 \pm$ Error %, $\mu s^n/\Omega$	$n_2 \pm$ Error %	$R_p \pm$ Error %, $M\Omega$	$CPE_1 \pm$ Error %, $\mu s^n/\Omega$	$n_1 \pm$ Error %	Chi ²	C_{CPE1} , μF	C_{CPE2} , μF	C_{exp} , μF
CoCr	0	87.4 ± 3.6				0.2 ± 6.5	14.7 ± 4.4	0.91 ± 1.16	0.0153	1.7		6.5
	7	44.6 ± 2.0				4.4 ± 4.1	8.2 ± 1.1	0.92 ± 0.25	0.0021	1.0		3.3
CoCrErGO	0	83.9 ± 1.3				2.3 ± 3.6	9.3 ± 1.1	0.90 ± 0.28	0.0017	0.6		3.9
	7	85.1 ± 0.5	2.3 ± 7.0	9.4 ± 0.6	0.90 ± 0.14	3.8 ± 12.8	10.1 ± 36.0	0.78 ± 8.90	0.0002		0.62	3.4
CoCrErGOHA	0	122.1 ± 0.6	0.3 ± 12.9	11.0 ± 1.2	0.90 ± 0.27	2.0 ± 6.7	6.6 ± 14.2	0.64 ± 5.21	0.0004		0.7	4.1
	7	125.6 ± 0.6	0.8 ± 27.9	9.4 ± 1.19	0.92 ± 0.27	11.0 ± 7.8	1.9 ± 15.0	0.71 ± 5.43	0.0004		1.0	3.9

In addition, the experimental capacitance values, C_{exp} , have been also calculated from the z'' values obtained at a high frequency of 1.58 kHz, following Equation (2):

$$C_{exp} = \frac{-1}{2\pi f z''} \quad (2)$$

For CoCr surfaces, after 7 days of immersion in PBS, the electrolyte resistance value, R_e (Table 1), is halved, indicating a higher quantity of ions in the medium during immersion time. On the other hand, the resistance due to the passive layer (R_p) is increased over the immersion time. This increase in resistance is accompanied by a slight decrease in the CPE values for bare CoCr surfaces immersed after 7 days. The analysis of the n exponent linked to the CPE ($n = 0.9$) in Table 1 allows us to calculate capacitance values (C_{CPE}) whose values are similar to those experimentally calculated (C_{exp}). The capacitance values can be nearly approximated with the response of the capacitor formed by the passive film.

The CoCrErGO surfaces immersed for 7 days deliver R_e values that remain constant with the testing time (Table 1). Comparing the R_p values between CoCrErGO and CoCr surfaces at 0 days of immersion, an increase of one order of magnitude in the resistance (R_p) is observed, indicating an improvement in the corrosion behavior due to the presence of ErGO. Nevertheless, at 0 days of immersion, the electrochemical system is still controlled by only one time constant (Figure 3a). However, after 7 days of immersion, the incorporation of a second time constant in the equivalent circuit is needed for the fitting of the impedance response that is associated with a greater contribution of the ErGO in the electrochemical response (Figure 3b). The resistance values, R_p , show a slight increase during immersion time but show similar values for CoCr surfaces at the same testing time. On the other hand, the shift of n exponent from 0.9 to 0.78 indicates that the system is moving away from a pure capacitive behavior. Instead of that, a new contribution appears, probably due to a diffusion process caused by the electrolyte movement from the solution bulk to the metal/ErGO interface.

The situation changes for CoCr surfaces with ErGO films functionalized with HA. In this case, the impedance response is dominated by two time constants from the beginning of the immersion (Figure 3b). In this case, the R_e value is higher than those obtained for CoCr and ErGO surfaces on the first day of immersion (Table 1) and remains constant until the end of testing. This increase could be related to the fact that the HA can be partially dissolved in the corrosive medium because it is not firmly linked to the ErGO. The resistance values of ErGOHA on CoCr surfaces (R_{coat}) increase somewhat during the immersion time, and the resistance attributed to the metal surface (R_p) follows the same trend. With respect to CPE values, CPE_2 , which is associated with the ErGOHA films, slightly decreases during the immersion time, and the n_2 exponent of 0.9 indicates that it can be considered as a quasicapacitance. The experimental capacitance values calculated in

a high-frequency region do not show significant differences as a consequence of immersion. However, CPE_1 , related to the metal/ErGOHA interface, shows values in the exponent n_1 from 0.64 to 0.71, for 0 and 7 days, respectively (Table 1), i.e., close to the ones expected for processes controlled by diffusion ($n = 0.5$). This result could reveal a diffusion process of the electrolyte through the ErGOHA. These results could be attributed to the adsorption of hyaluronic acid on the ErGO and be mainly due to the high hydration capacity of HA, i.e., its great ability to incorporate water molecules into its structure. The proportion of water in the HA structure can be 1000 times greater than its molecular weight. This fact makes the diffusion of not very bulky species through it feasible. However, other molecules with a higher volume, as is the case of some proteins, would be discarded in this diffusion process. The structure of HA changes constantly. Its conformation makes variable diffusion processes feasible that cause changes in n_2 over the immersion time. The functionalization of the ErGO surfaces with hyaluronic acid consists of an elongated conformation of the HA molecule forming a so-called polymer brush [21–23]. Such a brush can be pictured as a strongly hydrated and highly dynamic meshwork of polymer chains weakly stretched in the direction perpendicular to the surface [24,25]. This configuration confers high diffusion coefficients that provide beneficial effects in joint lubrication.

To summarize, CoCrErGO surfaces functionalized with HA do not change the corrosion resistance versus immersion time in PBS. However, these surfaces can be better prepared to support the wear process in replaced joints, providing great hydration capabilities together with lubrication. Both properties are potential characteristics for resisting the mechanical stress but can also induce other cell functions related to differentiation and the cell communication process.

An extension of this research, in order to investigate the potential use of this material for body implants, includes the study of biocompatibility, cytotoxicity, and inflammatory responses performed in macrophages, the main cells involved in the primary response to foreign bodies [14].

Figure 4 shows comparative optical microscopy images of macrophages cultured over 72 h on discs of CoCrErGOHA, CoCrErGO, and CoCr. The distribution of cells on each surface reveals differences in material biocompatibility upon surface modification. On the CoCr surfaces, the macrophages show a heterogeneous distribution over the surface, showing cells clumps in some areas of the material (Figure 4a). ErGO modification on the CoCr surfaces induces changes in the distribution of the cells (Figure 4b) as macrophages appear quite uniformly distributed. Additional functionalization of CoCrErGO surfaces with HA (Figure 4c) causes an observable increase in the number of macrophages, a sign that could suggest an improvement in the biocompatibility of the material upon HA functionalization. Cells show a relatively homogenous distribution on this surface, although some cells are accumulated in clusters.

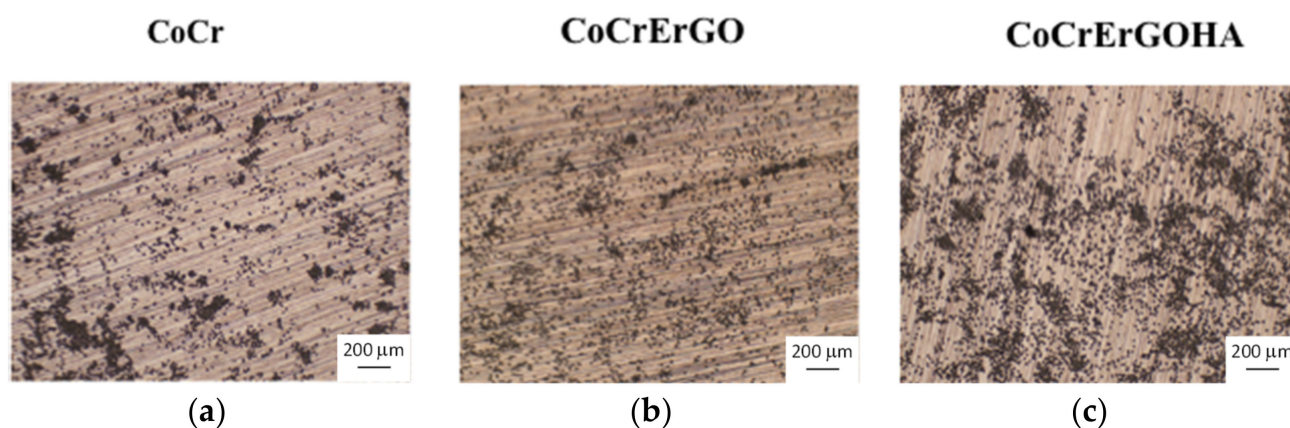


Figure 4. Optical microscopy: Pattern distribution of macrophages J774A.1 on CoCr (a), CoCrErGO (b), and CoCrErGOHA (c) discs after 72 h in culture.

To analyze the biocompatibility of CoCrErGOHA, CoCrErGO, and CoCr discs, a comparative analysis of the proliferation of macrophages has been performed. Proliferation has been measured by the cleavage of the tetrazolium salt WST-1 to formazan by cell mitochondrial dehydrogenases. The increase in enzyme activity leads to an increase in the amount of formazan dye formed, a compound that gives an increase in absorbance, which directly correlates with the number of metabolically active cells in the culture.

Figure 5 shows the absorbance as a measure of cell proliferation and viability of macrophages, cultured for 72 h on CoCrErGOHA, CoCrErGO, and CoCr surfaces. Cells without any material have been included here as a control to measure the maximum proliferation for this assay (Figure 5). As Figure 5 shows, a comparable macrophage proliferation is observed on CoCr and CoCrErGO surfaces, as non-significant differences were observed in ErGO deposition on CoCr. However, statistically significant differences in the macrophage proliferation and viability are obtained when the surface is additionally functionalized with HA (Figure 5). Although the proliferation is not as high as the one observed in the absence of material (control), the functionalization of CoCrErGO with HA seems to improve the viability of the macrophages as a high proliferation rate was observed, suggesting the greater biocompatibility of this material.

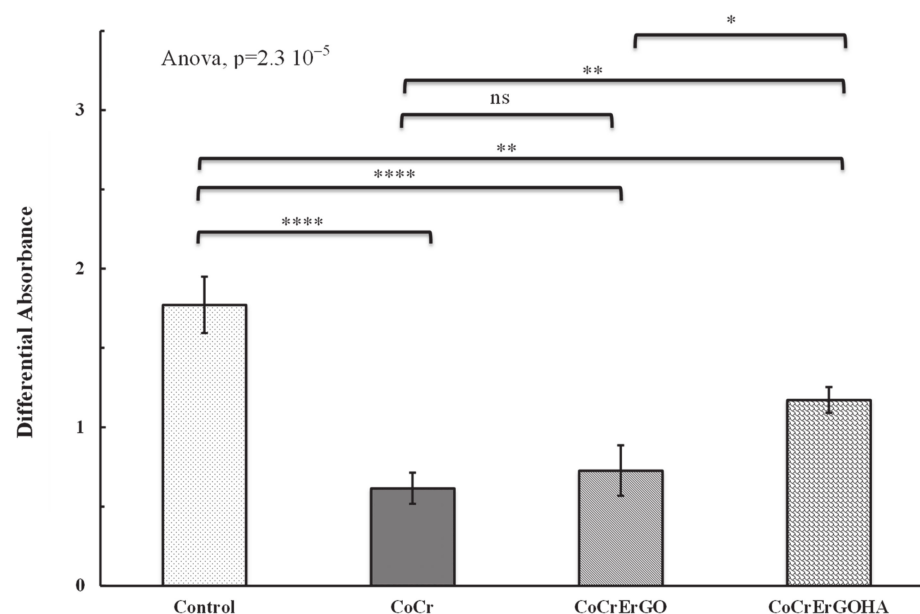


Figure 5. Effect of CoCr, CoCrErGO, and CoCrErGOHA surfaces on the proliferation and viability of macrophages' J774A.1 cultures. Macrophages were also cultured in the absence of any discs, used as a control. Differences were significant at p value ≤ 0.05 (*: $p \leq 0.05$, **: $p \leq 0.01$ and ****: $p \leq 0.0001$) and values with $p > 0.05$ were considered non significant (ns).

To further confirm the improvement in the viability observed upon functionalization of CoCrErGO with HA, the LDH/WST-1 activity ratio has been measured here for each material as a biocompatibility index. This ratio relates cell death to the number of metabolically active cells [12]. Cell death has been measured from the LDH activity, and the number of metabolically active cells has been measured from the proliferation results observed in the WST-1 assay. The LDH/WST-1 ratio (Figure 6) shows a small value when culture viability is good, as shown here by the control sample in the absence of any material, and a major value as the viability of the culture decays. The value of the LDH/WST-1 ratio for the CoCrErGOHA surfaces (Figure 6) is smaller than the values shown by the CoCr and CoCrErGO samples, suggesting better biocompatibility upon HA functionalization. The differences observed between the materials analyzed do not reach statistically significant levels.

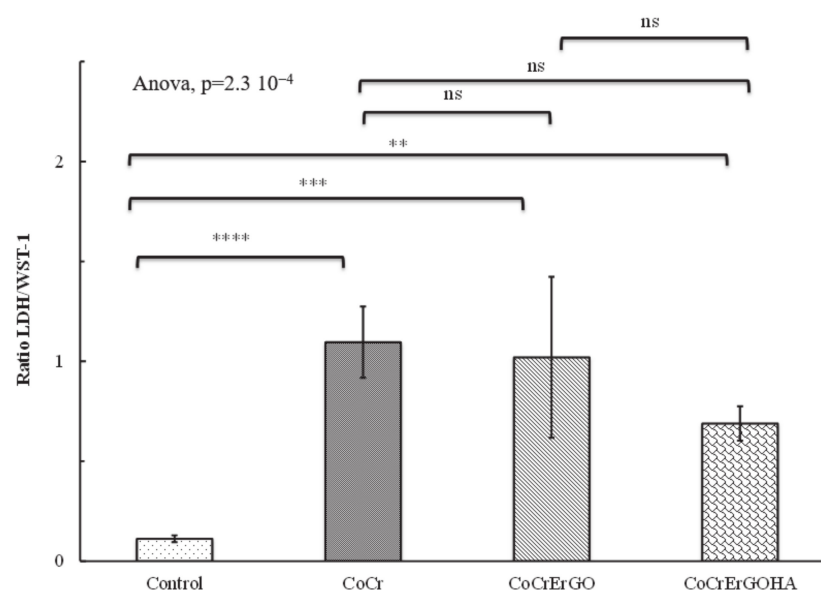


Figure 6. Effect of CoCr, CoCrErGO, and CoCrErGOHA surfaces in the LDH/WST-1 activity ratio as a measurement of macrophages' J774A.1 citocompatibility. Macrophages were also cultured in the absence of any discs, used here as a control (Cells). Differences were significant at p value ≤ 0.05 (**: $p \leq 0.01$, ***: $p \leq 0.001$ and ****: $p \leq 0.0001$) and values with $p > 0.05$ were considered non significant (ns).

The inflammatory response is studied by the quantification of two cytokine representatives of the inflammatory response, such as TNF- α and IL-10, mediators of the pro-inflammatory and the anti-inflammatory response, respectively [26]. The two cytokines have been quantified in supernatants after exposure of macrophages cultures to the materials for 72 h. As can be seen in Table 2, CoCrErGOHA and CoCrErGO surfaces show higher concentrations of TNF- α in comparison with the values shown by CoCr in the absence of any material. The increase in TNF- α levels could be related to a pro-inflammatory response activated by the ErGO present on both CoCrErGOHA and CoCrErGO surfaces. However, the analysis of the concentration of an anti-inflammatory cytokine, such as IL-10, in these samples seems to indicate a beneficial change in the inflammatory response with the additional HA functionalization of CoCrErGO. The comparative analysis of IL-10 in the supernatants analyzed shows a higher value of this anti-inflammatory cytokine in the CoCrErGOHA samples that is higher than those obtained in CoCr and CoCrErGO surfaces and similar to the levels shown in the absence of any material. This result suggests an improvement in the inflammatory behavior on the functionalization with HA of CoCrErGO surfaces.

Table 2. Concentration of TNF- α (pg/mL) and IL-10 (pg/mL) in the supernatants of macrophages cell cultured for 72 h in the presence of different modified surfaces. In (), there are the \pm SD values. The data are the mean results of three different independent assays; each one of which has an independent triplicate for each sample.

Cytokines	No Material	CoCr	CoCrErGO	CoCrErGOHA
TNF- α	96.73 (± 11.3)	80.46 (± 12.6)	110.34 (± 50.4)	130.28 (± 11.1)
IL-10	160.97 (± 31.9)	85.21 (± 61.6)	84.65 (± 43.3)	139.44 (± 60.6)
TNF- α /IL-10	0.61	0.94	1.30	0.93

Although the differences in TNF- α and IL-10 are not statistically significant (data not shown), an analysis of the balance between pro-inflammatory versus anti-inflammatory [27] response has been carried out here. This inflammatory balance is measured for each material by the ratio between TNF- α and IL-10 values. As can be seen in Table 2, CoCrErGO

surfaces show the highest value of TNF- α /IL-10 ratio, a result that can be related to the fact that micro-sized GO could cause serious inflammatory responses, demonstrated by a remarkable increase of IL-6, TNF- α , MCP-1 IL-12, and IFN- γ [28,29]. Besides this, Ma et al. [30] proposed that larger GO could induce more inflammatory cytokines by interacting with toll-like receptors and activating an NF-kB pathway. Nevertheless, the functionalization of CoCrErGO with HA breaks this tendency, as a ratio of TNF- α /IL-10 comparable to the one shown by the CoCr (0.93 versus 0.94, respectively) was observed. According to the study by Kiew and co-workers [31], nanomaterials with a more hydrophilic surface and a controlled size of approximately 150 nm could avoid being recognized by macrophages through the weakening of the opsonin–protein interaction. Therefore, surfaces functionalized with more hydrophilic compounds, as in the case of CoCrErGOHA surfaces, seem to be suitable candidates for avoiding inflammatory responses. The HA functionalization of CoCrErGO has an optimal concentration that provides an effective boundary lubricant on the retrieved CoCr femoral head surface [32]. The optimal HA concentration was close to the physiological concentration (i.e., 3–4 mg/mL) in the human synovial fluid. Thus, HA concentrations that are lower or higher than the physiological range resulted in a decrease in the effectiveness of boundary lubrication [13]. This result might be caused by the low adsorption of HA on the CoCr femoral head surface at a low HA concentration and the high viscosity of HA when the concentration of HA is high.

4. Conclusions

The ErGO on CoCr surfaces functionalized with HA shows high hydration and diffusion capacity without affecting the corrosion resistance in the physiological PBS medium over time.

An improvement in the biocompatibility of the material upon HA functionalization produced an increase in the number of macrophages and higher homogenous distribution on the material surface.

Functionalization with HA of ErGO on CoCr improves the inflammatory response of CoCrErGO.

Author Contributions: Conceptualization, B.T.P.-M., B.C., M.L.E., M.C.G.-A., and R.M.L.; methodology, B.C., B.T.P.-M., S.S.J., M.L.E., M.C.G.-A., and R.M.L.; software, B.T.P.-M., B.C., M.L.E., M.C.G.-A., R.M.L., and S.S.J.; validation, B.T.P.-M., B.C., M.L.E., M.C.G.-A., and R.M.L.; formal analysis, B.T.P.-M., B.C., S.S.J., M.L.E., M.C.G.-A., and R.M.L.; investigation, B.T.P.-M., B.C., M.L.E., M.C.G.-A., and R.M.L.; resources, B.T.P.-M., M.L.E., M.C.G.-A., and R.M.L.; data curation, B.T.P.-M., B.C., M.L.E., M.C.G.-A., and R.M.L.; writing—original draft preparation, B.C., M.L.E., M.C.G.-A., and R.M.L.; writing—review and editing, B.C., M.L.E., M.C.G.-A., and R.M.L.; visualization, B.C., M.L.E., M.C.G.-A., and R.M.L.; supervision, B.C., M.L.E., M.C.G.-A., and R.M.L.; project administration, B.T.P.-M., M.L.E., M.C.G.-A., and R.M.L.; funding acquisition, B.T.P.-M., M.L.E., M.C.G.-A., and R.M.L. All authors have read and agreed to the published version of the manuscript.

Funding: Financial support received through the RTI2018-101506-B-C31 and RTI2018-101506-B-C33 from the Ministerio de Ciencia, Innovación y Universidades (MICIU/FEDER), and through the MAT2015-67750-C3-2-R, MAT2015-67750-C3-1-R from the Ministerio de Economía y Competitividad (MINECO/FEDER) from Spain.

Acknowledgments: The authors wish to thank Guillermo Padilla PhD (G.P.) from the Bioinformatics and Biostatistics facility at Centro de Investigaciones Biológicas, CIB-CSIC, for technical assistance in the statistical analysis of macrophages data.

Conflicts of Interest: There are no conflicts of interest to declare. The authors will receive no benefit of any kind either directly or indirectly.

References

1. Eliaz, N. Corrosion of Metallic Biomaterials: A Review. *Materials* **2019**, *12*, 407. [[CrossRef](#)]
2. Mischler, S.; Muñoz, A.I. Wear of CoCrMo Alloys Used in Metal-on-Metal Hip Joints: A Tribocorrosion Appraisal. *Wear* **2013**, *297*, 1081–1094. [[CrossRef](#)]

3. Bijukumar, D.R.; Segu, A.; Souza, J.C.M.; Li, X.; Barba, M.; Mercuri, L.G.; Jacobs, J.J.; Mathew, M.T. Systemic and Local Toxicity of Metal Debris Released from Hip Prostheses: A Review of Experimental Approaches. *Nanomed. Nanotechnol. Biol. Med.* **2018**, *14*, 951–963. [\[CrossRef\]](#)
4. Ingham, E.; Fisher, J. The Role of Macrophages in Osteolysis of Total Joint Replacement. *Biomaterials* **2005**, *26*, 1271–1286. [\[CrossRef\]](#) [\[PubMed\]](#)
5. Nich, C.; Goodman, S.B. Role of Macrophages in the Biological Reaction to Wear Debris from Joint Replacements. *J. Autom. Inf. Sci.* **2014**, *24*, 259–265. [\[CrossRef\]](#)
6. Wimmer, M.A.; Sprecher, C.; Hauert, R.; Täger, G.; Fischer, A. Tribochemical Reaction on Metal-on-Metal Hip Joint Bearings: A Comparison between in-Vitro and in-Vivo Results. *Wear* **2003**, *255*, 1007–1014. [\[CrossRef\]](#)
7. Mathew, M.T.; Nagelli, C.; Pourzal, R.; Fischer, A.; Laurent, M.P.; Jacobs, J.J.; Wimmer, M.A. Tribolayer Formation in a Metal-on-Metal (MoM) Hip Joint: An Electrochemical Investigation. *J. Mech. Behav. Biomed. Mater.* **2014**, *29*, 199–212. [\[CrossRef\]](#) [\[PubMed\]](#)
8. Liao, Y.; Pourzal, R.; Wimmer, M.A.; Jacobs, J.J.; Fischer, A.; Marks, L.D. Graphitic Tribological Layers in Metal-on-Metal Hip Replacements. *Science* **2011**, *334*, 1687–1690. [\[CrossRef\]](#) [\[PubMed\]](#)
9. Zhu, Y.; Murali, S.; Cai, W.; Li, X.; Suk, J.W.; Potts, J.R.; Ruoff, R.S. Graphene and Graphene Oxide: Synthesis, Properties, and Applications. *Adv. Mater.* **2010**, *22*, 3906–3924. [\[CrossRef\]](#)
10. Zhang, W.; Lee, S.; McNear, K.L.; Chung, T.F.; Lee, S.; Lee, K.; Crist, S.A.; Ratliff, T.L.; Zhong, Z.; Chen, Y.P.; et al. Use of Graphene as Protection Film in Biological Environments. *Sci. Rep.* **2014**, *4*, 4097. [\[CrossRef\]](#) [\[PubMed\]](#)
11. García-Argumán, A.; Llorente, I.; Caballero-Calero, O.; González, Z.; Menéndez, R.; Escudero, M.L.; García-Alonso, M.C. Electrochemical Reduction of Graphene Oxide on Biomedical Grade CoCr Alloy. *Appl. Surf. Sci.* **2019**, *465*, 1028–1036. [\[CrossRef\]](#)
12. Escudero, M.L.; Llorente, I.; Pérez-Maceda, B.T.; José-Pinilla, S.S.; Sánchez-López, L.; Lozano, R.M.; Aguado-Henche, S.; de Arriba, C.C.; Alobera-Gracia, M.A.; García-Alonso, M.C. Electrochemically Reduced Graphene Oxide on CoCr Biomedical Alloy: Characterization, Macrophage Biocompatibility and Hemocompatibility in Rats with Graphene and Graphene Oxide. *Mater. Sci. Eng. C* **2020**, *109*, 110522. [\[CrossRef\]](#)
13. Mazzucco, D.; Scott, R.; Spector, M. Composition of Joint Fluid in Patients Undergoing Total Knee Replacement and Revision Arthroplasty: Correlation with Flow Properties. *Biomaterials* **2004**, *25*, 4433–4445. [\[CrossRef\]](#)
14. Nich, C.; Takakubo, Y.; Pajarinen, J.; Ainola, M.; Salem, A.; Sillat, T.; Rao, A.J.; Raska, M.; Tamaki, Y.; Takagi, M.; et al. Macrophages—Key Cells in the Response to Wear Debris from Joint Replacements. *J. Biomed. Mater. Res. Part A* **2013**, *101*, 3033–3045. [\[CrossRef\]](#)
15. Perez-Maceda, B.; López-Fernández, M.; Díaz, I.; Kavanaugh, A.; Billi, F.; Escudero, M.; García-Alonso, M.; Lozano, R. Macrophage Biocompatibility of CoCr Wear Particles Produced under Polarization in Hyaluronic Acid Aqueous Solution. *Materials* **2018**, *11*, 756. [\[CrossRef\]](#) [\[PubMed\]](#)
16. Wang, J.; Witte, F.; Xi, T.; Zheng, Y.; Yang, K.; Yang, Y.; Zhao, D.; Meng, J.; Li, Y.; Li, W.; et al. Recommendation for Modifying Current Cytotoxicity Testing Standards for Biodegradable Magnesium-Based Materials. *Acta Biomater.* **2015**, *21*, 237–249. [\[CrossRef\]](#) [\[PubMed\]](#)
17. Lozano, R.M.; Pérez-Maceda, B.T.; Carboneras, M.; Onofre-Bustamante, E.; García-Alonso, M.C.; Escudero, M.L. Response of MC3T3-E1 osteoblasts, L929 fibroblasts, and J774 macrophages to fluoride surface-modified AZ31 magnesium alloy. *J. Biomed. Mater. Res. Part A* **2013**, *101*, 2753–2762. [\[CrossRef\]](#) [\[PubMed\]](#)
18. R Core Team. *R: A Language and Environment for Statistical Computing*; R Foundation for Statistical Computing: Vienna, Austria, 2020.
19. Brug, G.J.; van den Eeden, A.L.G.; Sluyters-Rehbach, M.; Sluyters, J.H. The Analysis of Electrode Impedances Complicated by the Presence of a Constant Phase Element. *J. Electroanal. Chem. Interfacial Electrochem.* **1984**, *176*, 275–295. [\[CrossRef\]](#)
20. Orazem, M.E.; Tribollet, B. Time-Constant Dispersion. In *Electrochemical Impedance Spectroscopy*; John Wiley & Sons, Ltd.: Hoboken, NJ, USA, 2008; pp. 233–263, ISBN 978-0-470-38158-8.
21. Horkay, F.; Basser, P.J.; Londono, D.J.; Hecht, A.-M.; Geissler, E. Ions in Hyaluronic Acid Solutions. *J. Chem. Phys.* **2009**, *131*, 184902. [\[CrossRef\]](#) [\[PubMed\]](#)
22. Baranova, N.S.; Nilebäck, E.; Haller, F.M.; Briggs, D.C.; Svedhem, S.; Day, A.J.; Richter, R.P. The Inflammation-Associated Protein TSG-6 Cross-Links Hyaluronan via Hyaluronan-Induced TSG-6 Oligomers. *J. Biol. Chem.* **2011**, *286*, 25675–25686. [\[CrossRef\]](#)
23. Richter, R.P.; Hock, K.K.; Burkhartsmeyer, J.; Boehm, H.; Bingen, P.; Wang, G.; Steinmetz, N.F.; Evans, D.J.; Spatz, J.P. Membrane-Grafted Hyaluronan Films: A Well-Defined Model System of Glycoconjugate Cell Coats. *J. Am. Chem. Soc.* **2007**, *129*, 5306–5307. [\[CrossRef\]](#)
24. De Gennes, P.-G. *Scaling Concepts in Polymer Physics*; Cornell University Press: Ithaca, NY, USA, 1979; ISBN 978-0-8014-1203-5.
25. Rubinstein, M.; Colby, R.H. *Polymer Physics*; Oxford University Press: Oxford, UK, 2003.
26. Murray, P.J.; Allen, J.E.; Biswas, S.K.; Fisher, E.A.; Gilroy, D.W.; Goerdt, S.; Gordon, S.; Hamilton, J.A.; Ivashkiv, L.B.; Lawrence, T.; et al. Macrophage Activation and Polarization: Nomenclature and Experimental Guidelines. *Immunity* **2014**, *41*, 14–20. [\[CrossRef\]](#) [\[PubMed\]](#)
27. Goswami, B.; Rajappa, M.; Mallika, V.; Shukla, D.K.; Kumar, S. TNF- α /IL-10 Ratio and C-Reactive Protein as Markers of the Inflammatory Response in CAD-Prone North Indian Patients with Acute Myocardial Infarction. *Clin. Chim. Acta* **2009**, *408*, 14–18. [\[CrossRef\]](#)

-
28. Qu, Y.; He, F.; Yu, C.; Liang, X.; Liang, D.; Ma, L.; Zhang, Q.; Lv, J.; Wu, J. Advances on Graphene-Based Nanomaterials for Biomedical Applications. *Mater. Sci. Eng. C* **2018**, *90*, 764–780. [[CrossRef](#)]
 29. Yue, H.; Wei, W.; Yue, Z.; Wang, B.; Luo, N.; Gao, Y.; Ma, D.; Ma, G.; Su, Z. The Role of the Lateral Dimension of Graphene Oxide in the Regulation of Cellular Responses. *Biomaterials* **2012**, *33*, 4013–4021. [[CrossRef](#)] [[PubMed](#)]
 30. Ma, J.; Liu, R.; Wang, X.; Liu, Q.; Chen, Y.; Valle, R.P.; Zuo, Y.Y.; Xia, T.; Liu, S. Crucial Role of Lateral Size for Graphene Oxide in Activating Macrophages and Stimulating Pro-Inflammatory Responses in Cells and Animals. *ACS Nano* **2015**, *9*, 10498–10515. [[CrossRef](#)] [[PubMed](#)]
 31. Kiew, S.F.; Kiew, L.V.; Lee, H.B.; Imae, T.; Chung, L.Y. Assessing Biocompatibility of Graphene Oxide-Based Nanocarriers: A Review. *J. Control. Release* **2016**, *226*, 217–228. [[CrossRef](#)] [[PubMed](#)]
 32. Park, J.-B.; Duong, C.-T.; Chang, H.-G.; Sharma, A.R.; Thompson, M.S.; Park, S.; Kwak, B.-C.; Kim, T.-Y.; Lee, S.-S.; Park, S. Role of Hyaluronic Acid and Phospholipid in the Lubrication of a Cobalt-Chromium Head for Total Hip Arthroplasty. *Biointerphases* **2014**, *9*, 031007. [[CrossRef](#)]